

See discussions, stats, and author profiles for this publication at: <https://www.researchgate.net/publication/228854133>

FAST and IMAGE–FUV observations of a substorm onset

Article · January 1344

DOI: 10.1029/2002JA009787

CITATIONS

82

READS

17

5 authors, including:



S. B. Mende

University of California, Berkeley

648 PUBLICATIONS 9,616 CITATIONS

[SEE PROFILE](#)



H. U. Frey

University of California, Berkeley

596 PUBLICATIONS 7,633 CITATIONS

[SEE PROFILE](#)



L. M. Peticolas

University of California, Berkeley

94 PUBLICATIONS 1,054 CITATIONS

[SEE PROFILE](#)



Nikolai Ostgaard

University of Bergen

159 PUBLICATIONS 1,457 CITATIONS

[SEE PROFILE](#)

Some of the authors of this publication are also working on these related projects:



ICON: the Ionospheric Connection Explorer [View project](#)



Ionospheric CONnection Explorer [View project](#)

All content following this page was uploaded by [H. U. Frey](#) on 25 April 2017.

The user has requested enhancement of the downloaded file. All in-text references [underlined in blue](#) are added to the original document and are linked to publications on ResearchGate, letting you access and read them immediately.

FAST and IMAGE-FUV observations of a substorm onset

S. B. Mende, C. W. Carlson, H. U. Frey, L. M. Peticolas, and N. Østgaard

Space Science Laboratory, University of California, Berkeley, Berkeley, California, USA

Received 19 November 2002; revised 14 May 2003; accepted 19 June 2003; published 12 September 2003.

[1] On 6 February 2002 the NASA FAST satellite transited a substorm break up arc approximately 1 min after substorm onset as identified by the NASA IMAGE satellite far ultraviolet (FUV) instrument complement. These IMAGE data show that both the intense electron and proton precipitation features seen by FAST were not present prior to substorm onset. The most intense onset poleward surge was produced by superthermal electrons, and their energy spectrum and field-aligned angular distribution were consistent with wave accelerated electrons. The low energy ion fluxes in the $\mathbf{E} \times \mathbf{B}$ direction and magnetometer measurements confirmed the presence of waves in this feature. Thus the leading edge of the auroral surge was not produced by quasi-static field-aligned currents and related “inverted V” electric fields. The onset arc was also the poleward boundary of intense energetic protons. The FUV proton auroral images indicate that substantial part of the ion energy was carried by protons of energy >25 keV. Equatorward of the surge, there was a broader region of electron precipitation with embedded quasi-static “inverted V” electric fields. The FAST particle and magnetometer measurements are consistent with a field-aligned current structure in which the bulk of the upward current was carried by the “inverted V” precipitation region. The region of the superthermal electrons carried very little net current. The high-density upward field-aligned current carried by the superthermal electrons was presumably balanced by oppositely directed downward currents carried by cold electrons. The ground onset location was separated from the closed/open field line boundary by an extended region of closed field lines. In this region there was some weak plasma sheet electron and proton precipitation, but there was no clear signature of any distant, prebreakup substorm onset activity. *INDEX TERMS:*

2704 Magnetospheric Physics: Auroral phenomena (2407); 2740 Magnetospheric Physics: Magnetospheric configuration and dynamics; 2716 Magnetospheric Physics: Energetic particles, precipitating; 2788

Magnetospheric Physics: Storms and substorms; 2736 Magnetospheric Physics: Magnetosphere/ionosphere interactions; *KEYWORDS:* auroral substorm, substorm onset, Alfvén-wave aurora, substorm onset precipitation

Citation: Mende, S. B., C. W. Carlson, H. U. Frey, L. M. Peticolas, and N. Østgaard, FAST and IMAGE-FUV observations of a substorm onset, *J. Geophys. Res.*, 108(A9), 1344, doi:10.1029/2002JA009787, 2003.

1. Introduction

[2] There is extensive evidence that the substorm expansion starts in the near-Earth region ($<8 R_e$) because substorm associated field dipolarizations are typically seen at geosynchronous altitude ($\sim 6.6 R_e$) [Cummings and Coleman, 1968; Cummings *et al.*, 1968; McPherron *et al.*, 1973] with associated energetic particle injections [e.g., DeForest and McIlwain, 1971; Mende *et al.*, 1972; McIlwain, 1974]. Ground-based optical and magnetic observations of substorm expansive phase phenomena also show that onset takes place on field lines that originate at latitudes lower than 67° [e.g., Akasofu, 1964; Akasofu and Meng, 1967; Akasofu, 1968; Nishida and Kokubun, 1971; Kisabeth and Rostoker, 1971]. These observations are somewhat consistent with a model in which the substorm is a spontaneous occurrence of current disruption (CD) [Lui, 1991; Lui *et al.*, 1991]. In this view the substorm starts near the Earth ($<8 R_e$)

by a localized instability mechanism that interrupts and diverts the cross tail current into the ionosphere via field-aligned currents.

[3] An alternative view is that during the substorm growth phase the field lines are distorted substantially and the field lines originating at latitudes lower than 67° latitude are stretched to $20 R_e$ and beyond. For example, the magnetic field which crosses the equator at $7.3 R_e$ at quiet time according to the Tsyganenko 1996 model could be stretched to $19.8 R_e$ during disturbed times [Lyons, 2000]. At substorm onset a near earth neutral line (NENL) is formed in the $\sim 20 R_e$ plasma sheet. The subsequent reconfiguration causes earthward plasma flow while the process propagates tailward [Hones, 1979; Hones and Schindler, 1979; Baker and McPherron, 1990]. In this view the generation of the substorm current wedge and associated current reconfiguration and the related low-latitude onset are consequences of the events initiating at $\sim 20 R_e$. In spite of its success at describing substorm phenomenology, this type of NENL model is not favored [Baker *et al.*, 1996] because of the evidence that current disruptions occur

$<10 R_e$, near the Earth [Ohtani *et al.*, 1988; Jacquey *et al.*, 1991] and that NENL line associated tailward flows occur exclusively beyond $\sim 20 R_e$ [Baumjohann *et al.*, 1990]. Connectivity between regions $<10 R_e$ and $\sim 20 R_e$ would require a severe stretching of the magnetic field. In a newer version of the NENL model the field line stretching is moderate and reconnection occurs at $X = \sim 20 R_e$ [e.g., Shiokawa *et al.*, 1997; Baker *et al.*, 1996; Baker *et al.*, 2002] and the resulting energetic plasma propagates earthward interacting with high-pressure plasma near Earth ($\sim 6\text{--}7 R_e$). The onset phenomena detectable from the ground occur as a consequence of this interaction somewhat later than the NENL formation and also nearer to the Earth.

[4] The two models, the NENL and the CD models, both involve magnetic field reconfiguration in the form of dipolarization which is topologically equivalent to the removal/disruption of current from the near-tail region of highly stretched field lines. The CD and NENL processes could be distinguished from each other by timing the onset as seen at some distance in the tail and comparing it with the timing of substorm events observed on the ground. P_{12} pulsation are often regarded as substorm onset time markers and fast plasma flows preceding P_{12} observations on the ground were reported by Sergeev *et al.* [1995] and Shiokawa *et al.* [1998]. However, P_{12} onsets are not necessarily the best substorm indicators since they can be delayed from substorm onset and it is better to study the auroral brightening directly as a signature of substorm onset [Liou *et al.*, 1999].

[5] Ohtani *et al.* [1999] examined the relative timing of Geotail ($X = -30 R_e$) and GOES 9 geosynchronous satellite and ground-based magnetic field data and found that magnetotail reconnection occurs before the near-Earth effects, such as the auroral brightening at substorm onset. In another case study, Baker *et al.* [2002] showed that the Cluster satellites at $19 R_e$ see reconnection signatures about 8 min prior to an auroral onset of the substorm as determined by the IMAGE FUV instrument. Unfortunately, the mapping of distant events observed with high-altitude satellites to specific auroras and substorm onset regions is quite complex. Based on these observations it is still hard to make a clear case in favor of one or the other model.

[6] An important aspect of substorms is the change of the magnetospheric current configuration at onset. As a result of dipolarization and consequent interruption of the cross tail current, the magnetosphere drives an alternate path for the current through the ionosphere. This current wedge and the associated field line configuration change propagate tailward as represented by the substorm poleward expansion seen at low altitude. Inherent in this description is the idea that the magnetosphere drives the dawn-dusk current of the substorm either through the plasmasheet or through the ionosphere and the loop is completed via field-aligned currents. It is also implied that the large duskside upward field-aligned currents set up electrostatic potential drops. These accelerate electrons and cause “inverted V” type electron spectra measured at low altitudes and the bright aurora in the substorm surge. Thus the type of precipitation in the surge and its location relative to the field-aligned current region are important clues regarding the models.

[7] Dubyagin *et al.* [2003] presented FAST data just prior to substorm onset when the satellite was traversing an

auroral arc. As documented by an all-sky camera, the overpass occurred 2 min and 10 s prior to its breaking up. That arc was produced by low-energy electrons with a field-aligned pitch angle distribution. From the observed proton pressure profile and the field model calculations they argue that this arc at 64.4° latitude was very close to the isotropic boundary, and therefore the subsequent break up must have occurred on field lines stretching only to $8 R_e$.

[8] Observations of post onset phase substorm auroras with IMAGE and FAST showed several cases where the poleward edge of the substorm surge and corresponding wave accelerated superthermal electrons were very near to the boundary of open-closed field lines [Mende *et al.*, 2002, 2003]. As we have discussed, if the substorm surge and the boundary of open-closed field lines were close to each other in latitude then one could argue for the direct connectivity between the substorm surge ($<67^\circ$ in lat.) and the regions of weak B_z ($\sim 20\text{--}100 R_e$) where reconnection processes occur regularly. The observation of the auroral configuration immediately prior to, or at, onset can provide crucial information about the configuration of the field in the substorm process. Auroral particle and field observations regarding the nature of the onset aurora and the presence or absence of particle beams are other critical information for understanding substorms. By a fortuitous coincidence, the FAST satellite passed through the auroral region very near the instant of substorm onset on 6 February 2002. The observations allow us to interpret the FAST particle data in terms of the nature of the particle acceleration forces and the extent of the open-closed field line regions in the instantaneous field configuration of substorm onset. The auroral situation was identified from the simultaneous IMAGE observations.

2. Data Presentation

[9] On 6 February 2002 the Interplanetary Magnetic Field (IMF), as measured by ACE key parameter survey data, was quite variable fluctuating between ± 10 nT in the period preceding substorm onset at 0018:00 UT. The IMAGE FUV data during the entire substorm history are presented in Figure 1.

[10] The IMAGE FUV instrumentation consists of the Wideband Imaging Camera (WIC) and the Spectrographic Imager (SI). WIC observes the aurora in a broad band (140–170 nm) sensitive mainly to LBH N_2 and some NI lines. The SI-12 channel, one of the two channels of the Spectrographic Imager (SI), images Doppler shifted Lyman alpha to monitor the global scale proton precipitation by suppressing the intense (>10 kR) geocoronal Lyman alpha background, which would otherwise appear as an impenetrable diffuse background [Mende *et al.*, 2000]. The third channel, the SI-13 channel, has a 5 nm passband (full width at half maximum) centered on the auroral OI 135.6 nm line. In addition to this line, there are two components of LBH, which also lie within the passband and contribute to the instrument signal. The auroral emissions in this band are absorbed to a greater degree by molecular O_2 than the emissions sensed by the WIC instrument. The intercomparison of the intensity of the signal in the SI-13 and WIC channels during auroral observation can be used to provide information about the mean energy of the precipitating particles. For example, relatively large SI-13 to WIC

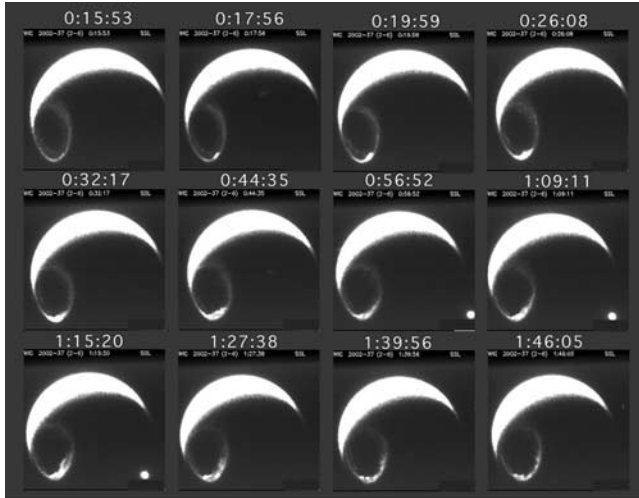


Figure 1. Overview of typical images of the substorm which started between 0013:50 and 0017:56 on 6 February 2002.

intensity ratios signify soft electron precipitation [Hubert *et al.*, 2002].

[11] The IMAGE FUV Wideband Imaging Camera (WIC) recorded the history of the substorm. In Figure 1 we illustrate the oval starting the sequence just before onset. Onset occurred sometime between frames 00:15:53 and 00:17:56 UT. The images were enhanced to intensify the

presubstorm faint oval. In order to maintain the same intensity scale, the substorm auroras were permitted to overload. The images do not represent the true dynamic range of the presubstorm and postsubstorm auroras. The image 0:15:53 was taken prior to onset and distinctly shows the presence of an equatorward arc around midnight. The postonset images (00:17:56 and later) show that the substorm auroral surge brightened and expanded in MLT, towards dusk and dawn. The onset of this substorm occurred over the mid-Atlantic, and the AL index responded gradually to this substorm with a more distinct peak later at about 0110:00 UT. It is evident from Figure 1 that after the onset a long period of intense auroral activity followed, covering >90 minutes until 0146:05 UT, consistent with a gradual decrease of the AL index by this time. After onset the auroral images depict typical substorm behavior with a fairly extended expansive phase. From the AL index and the IMAGE FUV data it is evident that this substorm was fairly typical, as a distinct and long lasting intensification of the global aurora. This substorm was preceded by other substorms and should not be regarded as an isolated substorm.

[12] Figure 2 presents all the FUV images near onset from 0015:53 to 0022:02 UT with the FAST satellite position (square box) and a small segment of the orbit track superposed. For each time the three images WIC, SI-12, and SI-13 are presented side by side from left to right. The onset is seen in the 00:17:56 WIC and SI-13 images. FAST detected the electron fluxes associated with the brightest substorm feature at 0018:40 UT. The sudden substorm intensification occurs on the equatorward side of the auroral oval. The intensifi-

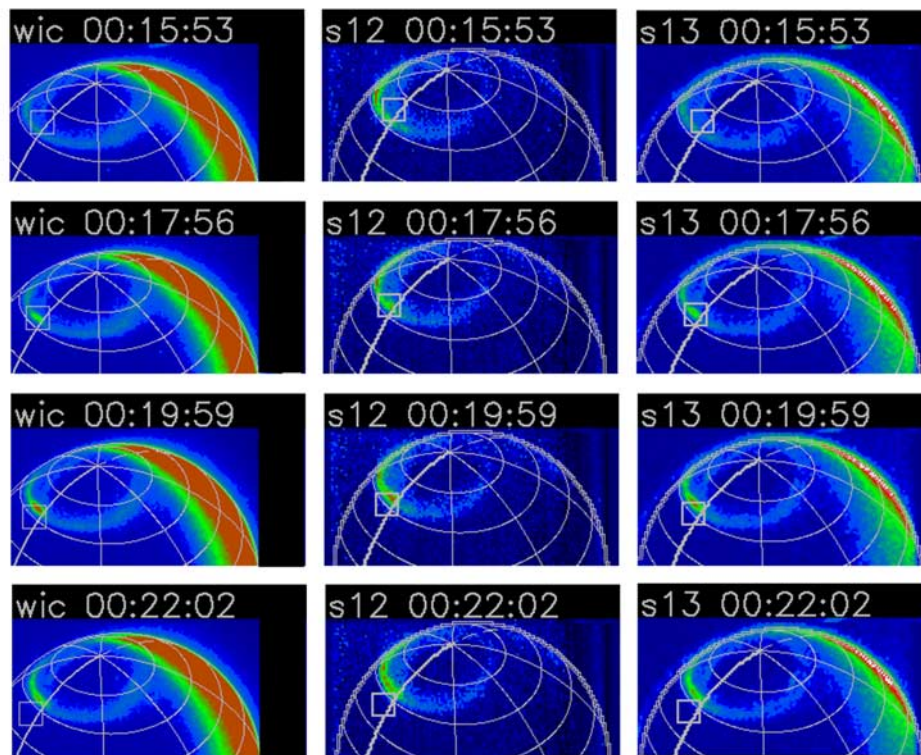


Figure 2. Detailed auroral morphology with superposed FAST satellite orbit track. Magnetic latitude of 30°, 45°, 60° and 75° and 0, 3, 6, 9, 12, 15, 18, 21 MLT grids are shown. The onset occurs just before (left) of the magnetic 0 meridian.

cation is only 2–3 degrees wide. It is embedded in a very faint auroral oval which is about 7–8° in latitude on the nightside. Although the proton aurora does not intensify to the same degree as the WIC and SI-13 signals, it also shows a broad oval of several degrees in width coincident with the overall electron dominated precipitation seen by WIC. The SI-12 data show a significant intensity enhancement between 0015:33 and 0017:56 UT and reaching maximum brightness at 0019:59 UT, showing that there was significant increase in proton precipitation at onset. The SI-13 image is similar to the WIC image except that the faint poleward part of the oval appears less distinct than in the WIC signal, which generally has superior signal to noise ratio. Thus the images provide the auroral context for the FAST observations and show that at 0018:40 UT the FAST satellite transited a substorm onset feature created before 0017:56 UT but after 0015:53 UT. The onset feature consisted of a significant temporal enhancement in both the electron and proton aurora. The images removed the space-time ambiguity normally present in in situ satellite observation.

[13] The FAST magnetic field, electron and ion data is given in Figure 3. Figure 3a shows magnetometer data, dB (nT), representing the detrended field vector perpendicular to the zeroth-order magnetic field and to the spacecraft velocity in field-aligned/spacecraft velocity coordinates; Figure 3b shows differential energy flux of electrons as a function of energy and time, averaged over the downward particles (pitch angles 0–50°); Figure 3c is the differential energy flux of electrons as a function of angle and time (electron pitch angle spectrogram), averaged over energies from 0.1 to 30 keV; Figure 3d is differential energy flux of ions as a function of energy and time, averaged over pitch angles in the loss cone (0–50°); Figure 3e is differential energy flux of ions as a function of angle and time (ion pitch angle spectrogram) averaged over energies from 0.5 to 24 keV; Figure 3f is a line plot of the precipitating energy flux of the electrons over energies from 0.1 to 30 keV and then mapped down to 100 km using the FAST-ionosphere magnetic field ratio from IGRF-95 in mW m^{-2} on a linear scale; Figure 3g is a line plot of the electron number flux treated the same way as Figure 3f but on logarithmic scale; Figure 3h is a line plot of the precipitating ion energy flux integrated over energies from 0.5 to 24 keV and then mapped down to 100 km using the magnetic field ratio; and Figure 3i is ion number flux integrated over energies from 0.5 to 24 keV and then mapped down to 100 km using the magnetic field ratio.

[14] The satellite moved from high latitude to lower latitude. The electron spectrogram data (Figure 3b) show that at latitudes above 70° (prior to 0016:40 UT) there are weak fluxes of few hundred eV electrons representing Polar Rain indicating that the satellite is in the polar cap. At 70.1° magnetic latitude the satellite encounters plasma sheet type precipitation of mean energy <1 keV and electron number fluxes of $>10^8 \text{ cm}^{-2} \text{ s}^{-1}$ (Figure 3g). Therefore this latitude is the open-closed field line boundary. These electrons also have isotropic pitch angle distributions with minimal up-going fluxes as depicted on the electron pitch angle spectrogram (Figure 3c). At about 64° the satellite encounters a very narrow region of intense electron flux (40–50 mW m^{-2} , Figure 3f) that exhibits the energy spectral character of superthermal electrons

(Figure 3b). These electrons also have very intense fluxes near zero pitch angle (Figure 3c). Similar soft electron precipitation is often seen in Alfvén wave dominated acceleration region [Chaston *et al.*, 2001, 2002]. Earthward propagating kinetic Alfvén waves have field-aligned electric field components that accelerate cold electrons and produce superthermal electron energy distribution with field-aligned, beam-like, pitch angle distribution [Chaston *et al.*, 2000]. It is emphasized that such wave accelerated electrons are not plasmasheet electrons but they are energized at about <1 R_e altitude above the aurora. Equatorward of these superthermal electrons and after a narrow region of lower intensity fluxes the satellite encounters a fairly weak inverted V-type peak (62° latitude) and then a very narrow region of diffuse precipitation extending to about 60° latitude. The pitch angle spectrogram (Figure 3c) shows that the electron precipitation is generally isotropic apart from the atmospheric loss cone in all regions, other than that of the wave accelerated electrons.

[15] The precipitating ion energy flux in Figure 3d shows banded weak ion fluxes appearing at $\sim 69^\circ$ in the higher energy channels. The more intense ion precipitation begins on the equatorward side of the oval starting at 64°, collocated with the very intense superthermal electron fluxes and the bright auroral feature. The ion precipitation extends further equatorward than the electrons. We can see intense ion precipitation between 64 and 61°, reaching $2\text{--}3 \times 10^7 \text{ cm}^{-2} \text{ s}^{-1}$ at three different places (Figure 3i). Note that the energy range of the FAST detector is limited to <30 keV and the proton spectrograms (Figure 3d) indicate that the energetic protons extend above the energy cutoff of the FAST analyzers at all locations in the plasma sheet from 61°–70°. The proton fluxes decrease at about 58 degrees as the satellite moves equatorward.

[16] In summary the FAST data clearly delineates the open/closed field line boundary, a region of closed field lines with weak ion fluxes poleward of the substorm surge, and a region of more intense ion precipitation equatorward and overlapping the location of the surge. The aurora at onset contains two distinct features: a very bright one, generated by wave accelerated superthermal electrons, and a separate less intense “inverted V” type aurora equatorward. Changes in the magnetic field data (dB) can be interpreted that the satellite passes through a time stationary sheet field-aligned current. In the Northern Hemisphere a negative change represents an upward current when the satellite moves equatorward. The magnetometer data shows that the equatorward inverted V-type aurora causes the largest dB in the data therefore this aurora carries the largest upward field-aligned current. There is also an upward current in the intense superthermal electron peak and the sharp gradients in the magnetometer data represent strong current densities; however the cumulative dB across this feature is relatively small, tending to support that the net field-aligned contribution of this region to the substorm field-aligned current system is small. The gap between the two auroral components is a region of downward current. The highest electron fluxes are encountered in the poleward part of the superthermal electron component with electron fluxes of $10^{11} \text{ electrons cm}^{-2} \text{ s}^{-1}$.

[17] The region indicated with broken vertical lines in Figure 3 was expanded and is shown as Figure 4. Figure 4a,

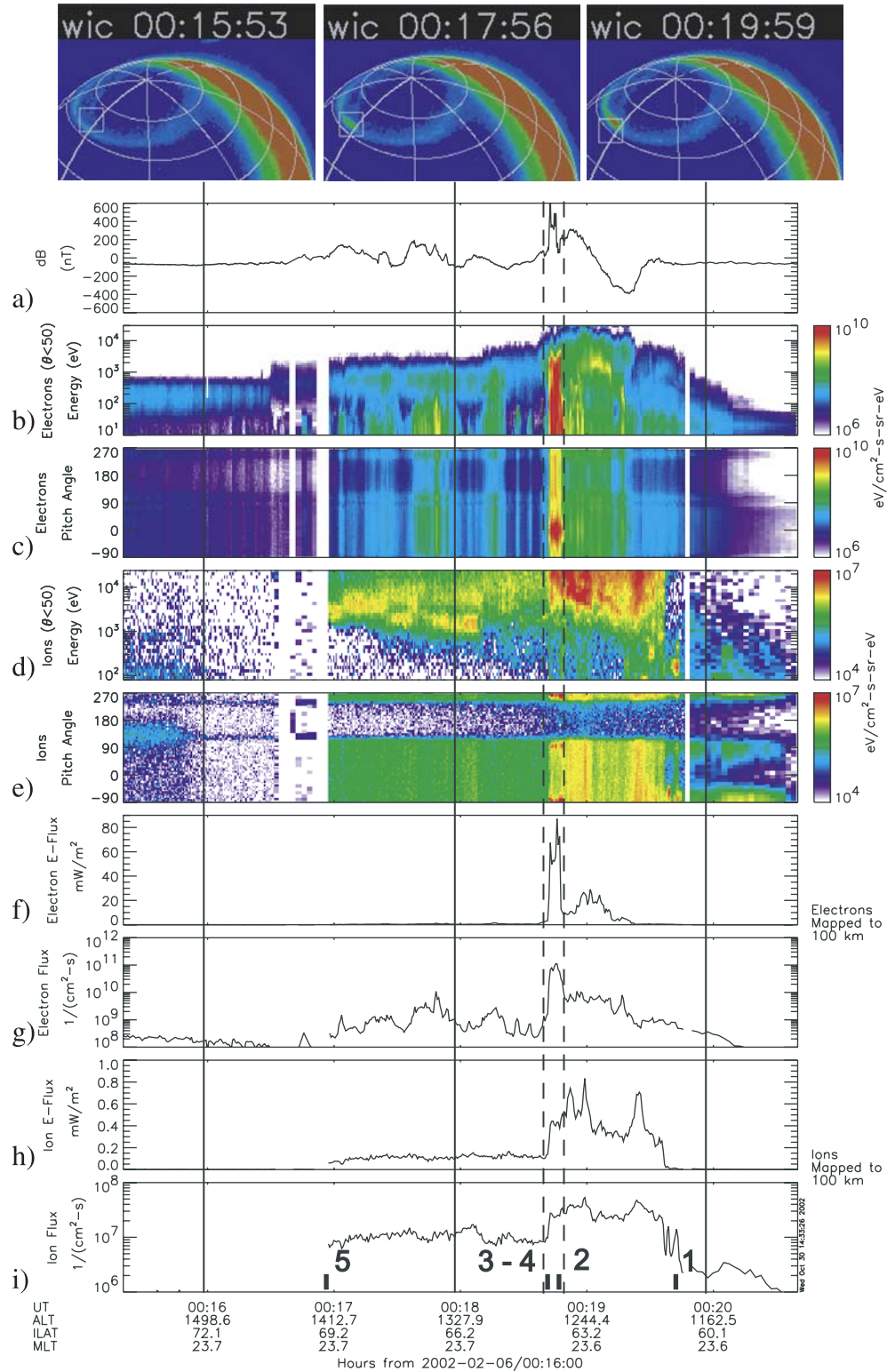


Figure 3. FAST data for orbit 21738. Magnetic field measurements (a), parallel electron spectrogram (b), electron pitch angle (c), parallel ion spectrogram (d), ion pitch angle (e), electron energy flux (f), electron number flux (g) ion energy flux (h) and ion number flux (i). Boundaries from field lines 1 to 5, identified in Figure 7, are marked on Figure 3i.

showing the precipitated electrons, was included to demonstrate the rich structure of the wave-accelerated electrons in the surge. Figure 4b, showing the pitch angle spectrogram of the electrons, demonstrates that the electrons are field-

aligned because they are most intense near 0° and 360° pitch angles. Figure 4c is the magnetometer data, plotted without the subtraction of the Earth field. Besides the large-scale feature (discussed in relation to Figure 3), the plot shows

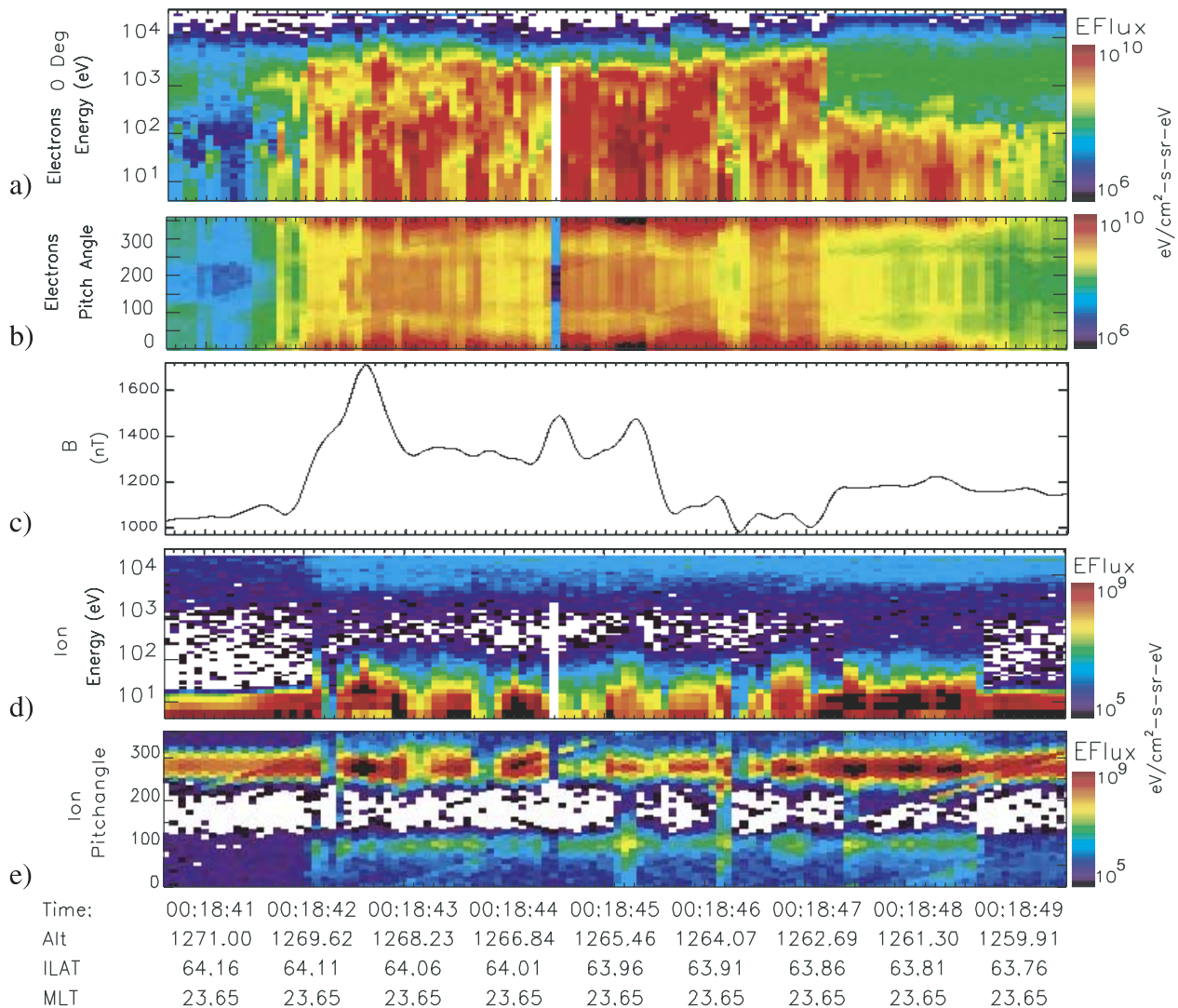


Figure 4. Expanded view (10 s) region of the FAST measurements indicated with broken vertical lines in Figure 3. (a) Energy spectrogram of the precipitated electrons; (b) the pitch angle spectrogram of the electrons; (c) the magnetometer data. Figures 4d and 4e are the ion energy and ion pitch angle spectrograms, respectively.

weak periodic modulation with about 0.6 to 0.8 s period. These modulations are direct signature of the waves. Figure 4d is the expanded version of the ion spectrogram (Figure 3d) with the energy range below 100 eV included. Figure 4e is the pitch angle spectrogram of the ions. These spectrograms also contain periodic intensifications of the particle energy fluxes in both figures. The pitch angle spectrogram shows the greatest intensity at 270° and less intensity at 90° . Figures 4d and 4e are consistent with ion flows in the $\mathbf{E} \times \mathbf{B}$ direction (270° pitch angle) driven by the Alfvén waves fields. The intensity of the observed ion flux depends on the motion direction of the satellite and the phase of the waves. In summary we can see direct evidence of the Alfvén waves in these low energy ion signatures.

[18] In the FUV images the two intense precipitating electron peaks appeared as a single feature, the bright substorm onset aurora. The distance between the two peaks was at the limit of resolution of the FUV cameras at this altitude in the IMAGE orbit. When mapped to the FAST

track, IMAGE sees the aurora where FAST was located at 0019:10 UT. This is to be compared with the actual intensity peak seen by FAST at 0018:40 UT. Our mapping is usually better than this (~ 250 km error) but this type of comparison is always subject to errors such as the motion of the aurora during the 2 min IMAGE cadence period.

[19] In Figure 5 we have plotted the IMAGE pixel intensities under the FAST track obtained during the FAST overpass. The WIC curve shows a slight enhancement between 0016:00 and 0016:30 UT which is close to the polar cap boundary. This enhancement is more pronounced in the SI-12 data indicating the presence of energetic protons. The SI-13 curve is noisier and it does not show an enhancement until 0018:00 UT. The large peak in all channels at 0019:10 UT is the substorm onset aurora. The proton peak is asymmetric with a larger enhancement poleward of the substorm bulge. In comparing the FAST particle data to optical data, one should recognize that there is about a latitude degree of charge exchange broadening in the optical proton aurora.

Although this charge exchange will spread the signal both poleward and equatorward, our view angle favored the poleward side in this observation.

[20] The higher flux energetic proton observation started at the same point as the electrons. However, based on the FAST data we cannot rule out the presence of higher-energy protons poleward of the substorm bulge because of the energy range limitation of the FAST detectors. Indeed the proton fluxes derived from the IMAGE SI-12 data (see below) are higher than seen by FAST. The presence of intense protons at the poleward boundary is in agreement with the observations that the protons lead the poleward expansion in the early phase of the substorm [e.g., *Mende et al.*, 2001].

[21] To facilitate a quantitative comparison between IMAGE and FAST, we interpreted and replotted the data of Figure 4 in Figure 5 using the IMAGE FUV calibration parameters derived from laboratory and in-flight calibration and Monte Carlo modeling [*Gérard et al.*, 2001; *Hubert et al.*, 2002]. The mean energy of the ions in the surge was probably above the FAST instrument measurement limit (Figure 3d). Thus we expect that the proton energy flux measured by FAST will be less than the value seen by IMAGE. The IMAGE derived proton energy flux was displayed as the Proton Eflux curve. It was obtained by smoothing the SI-12 detector counts with a 2.5 pixel wide filter. The peak value of 4 mW m^{-2} is higher than peak fluxes of $0.6\text{--}0.8 \text{ mW m}^{-2}$ derived from the FAST data (Figure 3h). Accordingly, the precipitated energy of the protons measured by IMAGE FUV was almost 6 times that measured by FAST.

[22] To compare the IMAGE FUV and FAST electron data, we subtracted SI-12 proton induced signal from the WIC and SI-13 channels and used the ratio of the resulting WIC to SI-13 ratio to obtain the mean energy of the electron precipitation. This technique was only applied to regions where the SI-13 counts were above 10 per pixel. This is displayed as “Mean e energy.” The curve, “Eflux from WIC” was obtained by dividing the observed and smoothed WIC counts by the counts which would be produced by a 1 mW m^{-2} energy flux of electrons with the mean energy represented by the “Mean e energy” curve. The optical data nicely confirms that the bulk of the aurora, coincident with the proton peak, is produced by electrons of mean energy of $\sim 0.5 \text{ keV}$ (see Figure 5). The peak of the precipitated energy obtained this way is about 10 mW m^{-2} . The FAST measurement of the peak of the precipitated electron energy flux was about 80 mW m^{-2} (Figure 3f). The dash-dotted black line on Figure 5 was obtained by smoothing the FAST electron energy flux curve with a time constant of 1 min ($\sim 250 \text{ km}$). The resulting energy peak is in fair agreement with the one obtained from the optical measurements. In summary, the IMAGE and FAST electron measurements agree reasonably well. The discrepancy between the IMAGE and FAST proton measurements can be explained by assuming a substantial fluxes of energetic ($>30 \text{ keV}$) protons in the surge aurora.

[23] The FAST magnetometer shows that the magnitude of the measured “background” field component changes very little as FAST passes the region of the wave accelerated surge electrons (Figure 3a). Therefore the net dc current carried in the region of the wave accelerated electrons is

quite small. There is a significant electron flux (Figure 3g, $\sim 10^{11} \text{ cm}^{-2} \text{ s}^{-1}$) in the wave-accelerated surge aurora; however the current carried by these must be balanced by counter flowing cold electrons, which are not seen by FAST. The largest magnetic field component change is registered when the satellite crosses the region of the “inverted V” aurora. From this we can conclude that the most significant field-aligned current region is associated with the equatorward lying “inverted V” type auroras. From comparing WIC images 0017:56 and 0019:59 UT we obtained that the intensity of precipitation increased only 20% during the actual FAST overpass of the surge aurora. This is important because the above interpretation of the FAST magnetometer data assumes that the current features were stationary during the satellite overpass.

3. Discussion

[24] We have in situ and remote measurements of the onset of a moderate substorm, which gradually reached $AL = 400 \text{ nT}$ about 1 hour after onset. The IMF B_x was negative and B_y was positive. The B_z component was quite variable between -10 and $+10 \text{ nT}$, and it is possible that the onset was associated with one of the transitions in the B_z component. By a fortuitous coincidence, the FAST satellite transited the auroral region in a north-south direction reaching the substorm break up arc just about two minutes after substorm onset brightening.

[25] The combined IMAGE FUV and FAST data showed that at substorm onset, an arc was located along the equatorward side of the auroral oval while points poleward were in a region of plasma sheet precipitation and of closed field lines. From the IMAGE FUV data we could establish that the FAST over-flight of the intense substorm onset feature occurred about 2 min after substorm onset. The latitude of the initial brightening and the open-closed field line boundary were widely separated. FAST traveled through this region immediately before onset and measured weak proton and electron fluxes, which were consistent with the faint preonset diffuse aurora seen by IMAGE in this region. The onset arc consisted of highly intense wave accelerated electrons carrying a large part of the auroral energy. FAST encountered energetic ions simultaneously with the intense onset feature. Following the intense auroral superthermal electrons FAST passed an auroral region of moderately intense precipitation of “inverted V” type accelerated electrons and associated field-aligned currents.

[26] The substorm onset manifested itself primarily by the sudden injection of intense waves and protons. The electrons in the surge are a product of the waves that accelerate the ionospheric electrons at relatively low altitudes in the ionosphere. As a result, the combined current carried by the wave accelerated electrons and by the return currents immediately adjacent to them is quite low.

[27] High-resolution ground-based studies of *Deehr and Lummerzheim* [2001] showed that in the presubstorm arc system, a pulse of increased electron number flux with an average energy of $<100 \text{ eV}$ precedes substorm onset. This occurred during auroral fading period immediately before onset. Field-aligned soft electrons were also seen by *Dubyagin et al.* [2003] in an arc prior to break up. The relatively low spatial resolution IMAGE instrumentation

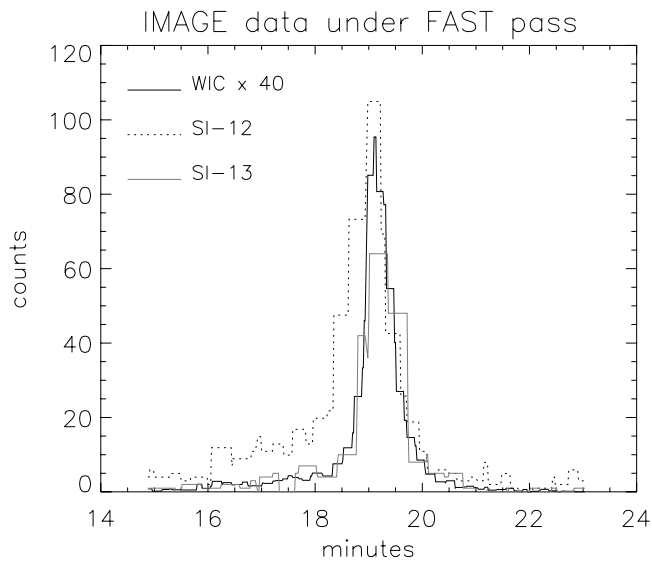


Figure 5. IMAGE FUV data pixel intensity under the FAST projected orbit track. The IMAGE data is taken with 2-min repetition rate. Two-minute orbit segments were taken from each appropriate image and were assembled into the above plot. The time coordinate should be interpreted as the geographic position of FAST at the time the IMAGE data was taken. The curves represent WIC, SI-12 (protons), and SI-13, respectively. Ordinates are in counts for SI-12 and SI-13 and in AD-units divided by 40 for WIC.

would not be able to observe the detailed dynamics of auroras created by these electrons and protons at onset and we cannot comment on the results of *Deehr and Lummerzheim* [2001]. However, the wave-accelerated soft electrons seen by them might be a precursor of the onset surge reported here.

[28] Our observations can be interpreted in terms of the illustration of Figure 7. The various magnetospheric/auroral regions are illustrated with different colors. The first region encountered by FAST is the Polar Cap region of open field lines signified by polar rain. The boundary separating the Polar Cap region from the next region is the open-closed field line Boundary. The last closed field line is labeled field line 5 and stretches to the distant tail. This is the location of the reconnection associated with steady state convection. Next was a region of highly stretched closed field lines with low-intensity plasmasheet boundary layer electron and weak proton precipitation, illustrated in blue in Figure 7. The next region equatorward, illustrated in red, and separated by field line 4, usually consists of field lines containing intense energetic proton precipitation in the quiescent state of the magnetosphere. These protons are a permanent feature and are often present regardless of substorm conditions. The proton precipitation is produced by trapped ion fluxes isotropised by the highly stretched field lines. The detected onset region occurs at geomagnetic latitudes of $64\text{--}67^\circ$ mapping to about $6\text{--}10 R_c$ radial distance down the tail. However, models generally represent an average magnetic configuration, and they are not necessarily good descriptors of preonset instantaneous field configuration. The innermost region separated by the isotropic boundary (IB, field line 1) [Sergeev *et al.*, 1983] is usually devoid of precipitation

because the particles are trapped in well-behaved dipole-like magnetic field lines with minimal pitch angle change. These boundaries were identified in the FAST data and plotted at the top of Figure 3a. These precipitation regions can be put in context with the classification of auroral regions and their boundaries from DMSP satellite measurements [Newell *et al.*, 1996].

[29] As we have discussed above, there is a region of “inverted V” type precipitation with an associated large upward field-aligned current equatorward of the intense surge containing the “Alfvén wave” accelerated electrons. This region is presumably associated with the shear or divergence of the high-speed plasma convections resulting from the redistribution of the plasma. These convection flows are represented with white arrows in Figure 7 in the top view onset. The “inverted V fields” are the signatures of intense field-aligned currents that cannot be supported by normal B parallel conductivity without an increase in the field-aligned potential drop. In this view the “inverted V precipitation” represents currents impressed on the ionosphere by the magnetospheric convection dynamo.

[30] The net change in the magnetic field across the superthermal electron component was minimal, implying that local return currents, carried by cold electrons, balance the current carried by the electron flux. From our low-altitude observations it may be fundamentally impossible to discriminate between the proposed substorm models; nevertheless it is important to discuss whether our observations are consistent with them.

[31] The onset occurred in the red region poleward of the IB and in the midst of proton precipitation, as shown for example by *Samson et al.* [1992a, 1992b], *Takahashi and Fukunishi* [2001], and *Mende et al.* [2001]. In Figure 7

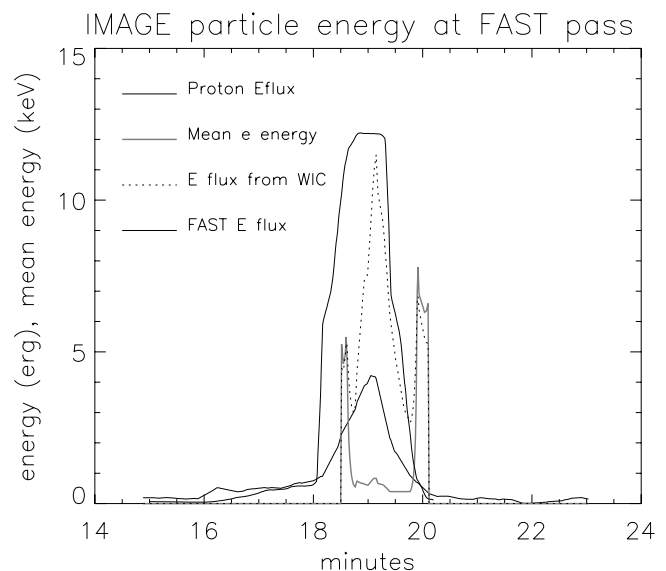


Figure 6. The IMAGE FUV data (Figure 4) replotted in terms of proton energy flux derived from the IMAGE SI-12 data in mWm^{-2} (thin black line), the mean energy of the electrons derived from the IMAGE WIC and SI-13 data in keV (wider grey line), the electron energy flux from WIC in mWm^{-2} (dashed), and the smoothed FAST electron energy flux in mWm^{-2} (dash dot line).

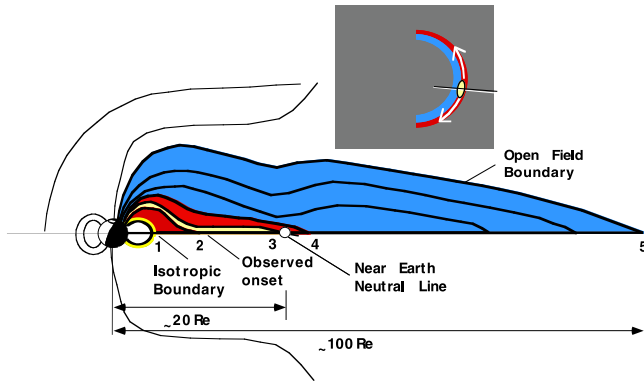


Figure 7. Summary sketch of the magnetospheric configuration. Field line 1 (61° ILAT) is at the isotropic boundary, field line 4 ($\sim 64^\circ$ ILAT) is the poleward boundary of the more intense proton precipitation, and field line 5 is the closed-open field line boundary ($\sim 70^\circ$ ILAT). The substorm auroral onset occurs between field lines 2 and 3 ($\sim 63.5\text{--}64^\circ$ ILAT). The onset is detected by the superthermal electrons that are accelerated by waves produced in the yellow region between field line 2 and 3. At the onset field line 3 coincides with the poleward boundary of the intense proton precipitation (field line 4). In the NENL model a neutral line occurs at about $20 R_e$ (indicated with white circle) that is either directly connected to the onset region (ILAT = 64° ILAT) by extreme stretching or the inward moving plasma moves across from field line 3 to 2. The onset would remain undetected on the ground until it reaches field line 2 in the $R \sim 5\text{--}8 R_e$ region (ILAT = 64° ILAT). With some modification this same sketch can be used to illustrate the current disruption CD model in which the current disruption occurs on field line 2 in the $5\text{--}8 R_e$ region and then propagates tail-ward and poleward. In all models, after onset the innermost field lines continue to dipolarize, gradually propagating the dipolarization activity toward higher latitudes. The top inset represents the view of the nightside auroral regions from above with a line representing the FAST pass.

we schematically illustrated the onset region in yellow, bounded by field lines 2 and 3. Our data does not rule out the possibility that during the substorm growth phase the plasma sheets thins radically until the outer field lines originating in this region stretch to $20 R_e$ down tail. The NENL would then form at about $20 R_e$ and fast earthward plasma flow would take place with associated magnetic field line motion and consequent dipolarization. As the magnetic field change propagates down along the field line it would launch Alfvén waves that produce intense wave accelerated electrons. Thus the mapping of the region between field line 2 and 3 is the substorm surge containing the beam-like superthermal electrons.

[32] The simultaneously appearing high-energy ions are probably part of the high-speed plasma flow itself that has undergone pitch angle randomization through the field dipolarization. These ions show isotropic pitch angle distribution at FAST altitude. After onset as the flow continues, more magnetic flux is driven in and piles up, adding to the flux in the near dipolar configuration at the

expense of the flux in the highly distorted closed field line regions. Thus the substorm surge is observed to exhibit poleward expansion. Our observations, namely the location of the onset, the presence of intense wave accelerated electrons near onset at fairly low latitudes and the relatively large distance between the onset and the open-closed field line boundary, agrees with the topology described herein.

[33] In the above model we implied that the field lines were highly stretched just prior to substorm onset and that the onset region was temporarily connected to the NENL region. In newer versions of the NENL models [e.g., Shiokawa *et al.*, 1998; Birn *et al.*, 1999; Baker *et al.*, 2002] the NENL is formed on field lines that stretch further out than the onset region and following reconnection earthward plasma flow is produced. This flow propagates earthward in a region of distorted field lines. According to this NENL model as the flow encounters the dense plasma on relatively dipolar field lines nearer the Earth, the flow brakes [Shiokawa *et al.*, 1997] and the deceleration currents are set up [Haerendel, 1992]. The sense of these currents will enhance the dipolarization. According to this model the resulting activity would be the current generator producing the auroral field-aligned currents and the corresponding intense auroras. The underlying assumption is that the sudden appearance of the substorm current wedge is solely due to reconfiguration of “conventional” field-aligned currents and the associated auroras are due to “inverted V” electric fields. As we have seen, the substorm surge itself does not show the characteristic of “inverted V” precipitation and the location of the higher-intensity field-aligned currents is equatorward of the surge. From this latitudinal displacement we could interpret that the Alfvén waves are the foot prints of the reconnection region and the strong field-aligned currents are those of the flow breaking occurring closer to the earth.

[34] In addition FAST or IMAGE did not observe any precursor activity at higher latitudes prior to onset in the field line region where the NENL is supposed to form in the newer NENL model. Note that it is possible that IMAGE had missed some short lived brightening in this latitude range since it takes only one short exposure every 2 min.

[35] Alternately the activity could have started in the region $8\text{--}10 R_e$ and our data could be consistent with the CD model, provided that we postulate that Alfvén waves are injected at the point of current disruption. In the CD model as discussed by Lui *et al.* [1991], the current reconfiguration at onset plays a significant role. Our observation, that the surge and the quasi-dc field-aligned currents are not the same, opens up a question regarding their simultaneity or their timing.

[36] The event described in this paper can be regarded as a snapshot taken very close to substorm onset. In later substorm phases the intense wave-accelerated electron aurora still represents the poleward boundary of the auroral oval containing intense “inverted V” type electron precipitation and energetic protons [Mende *et al.*, 2003]. However in the later phases, the surge arc is located very close to the open-closed field-line boundary signifying that as the zone containing intense precipitation increased, the zone of highly distorted plasma sheet field lines located near the open-closed field-line boundary diminished. This is consis-

tent with the idea that the wave-produced electrons represent the field line dipolarization boundary and the poleward propagating surge.

[37] In summary, our data confirms that the onset consists of the sudden appearance of the wave accelerated electrons [Deehr and Lummerzheim, 2001]. These electrons represent the highest-energy density precipitation at onset. Since the magnetic field reconfiguration is the most likely source of the waves, it is probably the primary energy source. Thus the substorm surge is not the conventional quasi-static field driven aurora representing a return current through the ionosphere with its source in the magnetosphere. Instead the current is generated by intense Alfvén waves resulting directly from field line dipolarization or reconnection. By the interaction of the waves with cold electrons in the $\sim 1 R_e$ region the wave Poynting flux is converted into the energy of superthermal electrons. The near simultaneous appearance of the energetic protons suggests that the transportation of the protons is also the result of the dipolarization that had produced the Alfvén waves. The fact that the surge carries minimal net field-aligned current indicates that the surge itself is not a current diversion of a magnetospheric current through the ionosphere. In this view the primary effect is the Alfvén wave accelerated aurora, and not the onset of a strong field-aligned current. However we would also expect to see strong field-aligned currents and inverted V auroras shortly after the initial event as the ionosphere-magnetosphere system responds to the shears and divergences of the plasma convection driven by the magnetic reconfiguration.

4. Conclusions

[38] 1. In the early onset phase the substorm surge aurora is dominated by a very intense fluxes (10^{11} electrons $\text{cm}^{-2} \text{s}^{-1}$) of relatively soft, superthermal energy spectrum with a field-aligned pitch angle distribution, typical properties of Alfvén waves accelerated electrons. The presence of the waves in this feature was confirmed by the FAST low-energy ion fluxes observed in the $\mathbf{E} \times \mathbf{B}$ direction and by the magnetometer measurements. The feature was located on the poleward side of the more intense aurora.

[39] 2. The poleward edge of the surge is also the boundary of the higher-energy ions. The IMAGE FUV optical data suggests that there is a substantial ion component of energy >30 keV and that the ion fluxes double in precipitated intensity shortly after onset.

[40] 3. Equatorward of this feature the aurora consisted of quasi-static “inverted V” electric field generated auroras.

[41] 4. Both auroral features were associated with intense field-aligned currents. The magnetometer shows that there is a broad region of fairly intense, net upward current at the “inverted V” type auroral region. The electron flux shows that there is a high-density field-aligned upward current carried by the Alfvén wave accelerated electrons, but the net current carried by this feature is minimal; presumably the current is cancelled by cold upward flowing electrons. These downward currents were not seen in the particle data because they were presumably carried by very low-energy upward flowing electrons. Thus the currents in the region of the superthermal electrons close locally and this region contributes minimally to the large-scale magnetospheric substorm current system.

[42] 5. An extended region of closed field lines with plasma sheet precipitation separated the ground onset point from the closed-open field-line boundary at the early stage of substorm development. Thus the field line containing substorm onset auroral brightening is at a great distance from the quiescent closed-open field-line boundary, where the steady state, nonsubstorm related convective field line reconnection takes place.

[43] 6. There is no clear signature of magnetic or of precipitating particle activity at low altitude in the region of closed field lines poleward of the onset point that would indicate that the NENL reconnection had occurred in this region prior to the onset seen in the aurora.

[44] **Acknowledgments.** The IMAGE FUV instrument is a complex system involving the work of many people at a large number of institutions. The authors would like to acknowledge their gratitude to the entire IMAGE development and operations team for the dedicated support of the FUV instrument science. The authors would like to acknowledge N. Ness at Bartol Research Institute for the ACE key parameter magnetic field data. This work was supported through SWRI subcontract 83820 at the University of California, Berkeley and by NASA under contract NAS5-96020. The FAST project data analysis is supported under NASA grant NAG5-3596.

[45] Arthur Richmond thanks the reviewers for their assistance in evaluating this paper.

References

- Akasofu, S. I., The development of the auroral substorm, *Planet Space Sci.*, **12**, 273, 1964.
- Akasofu, S. I., *Polar Magnetospheric Substorms*, D. Reidel, Norwell, Mass., 1968.
- Akasofu, S. I., and C.-I. Meng, Polar magnetic substorm in the evening sector, *J. Atmos. Terr. Phys.*, **29**, 1127, 1967.
- Baker, D. N., and R. L. McPherron, Extreme energetic particle decreases near geostationary orbit: A manifestation of current diversion within the inner plasma sheet, *J. Geophys. Res.*, **95**, 6591, 1990.
- Baker, D. N., T. I. Pulkkinen, V. Angelopoulos, W. Baumjohann, and R. L. McPherron, Neutral line model of substorms: Past results and present view, *J. Geophys. Res.*, **101**, 12,975, 1996.
- Baker, D. N., et al., Timing of magnetic reconnection initiation during a global magnetospheric substorm onset, *Geophys. Res. Lett.*, **29**(24), 2190, doi:10.1029/2002GL015539, 2002.
- Baumjohann, W., G. Paschmann, and H. Luhr, Characteristics of high-speed ion flows in the plasma sheet, *J. Geophys. Res.*, **95**, 3801, 1990.
- Birn, J., M. Hesse, G. Haerendel, W. Baumjohann, and K. Shiokawa, Flow braking and the substorm wedge, *J. Geophys. Res.*, **104**, 19,895, 1999.
- Chaston, C. C., C. W. Carlson, R. E. Ergun, and J. P. McFadden, Alfvén waves, density cavities and electron acceleration observed from the FAST spacecraft, *Phys. Scripta*, **T84**, 64, 2000.
- Chaston, C. C., W. J. Peria, C. W. Carlson, R. E. Ergun, and J. P. McFadden, FAST observations of inertial Alfvén waves and electron acceleration in the dayside aurora, *Phys. Chem. Earth*, **26**, 201, 2001.
- Chaston, C. C., J. M. Bonnel, L. M. Peticolas, C. W. Carlson, R. E. Ergun, and J. P. McFadden, Driven Alfvén waves and electron acceleration: A FAST case study, *Geophys. Res. Lett.*, **29**(11), 1535, doi:10.1029/2001GL013842, 2002.
- Cummings, W. D., and P. J. Coleman, Magnetic fields in the magnetopause and vicinity at synchronous altitude, *J. Geophys. Res.*, **73**, 5699, 1968.
- Cummings, W. D., J. N. Barfield, and P. J. Coleman, Magnetospheric substorms observed at the synchronous orbit, *J. Geophys. Res.*, **73**, 6687, 1968.
- Deehr, C., and D. Lummerzheim, Ground based optical observations of hydrogen emission in the auroral substorm, *J. Geophys. Res.*, **106**, 33, 2001.
- DeForest, S. E., and C. E. McIlwain, Plasma clouds in the magnetosphere, *J. Geophys. Res.*, **76**, 3587, 1971.
- Dubyagin, S. V., V. A. Sergeev, C. W. Carlson, S. R. Marple, T. I. Pulkkinen, and A. G. Yahnin, Evidence of near earth break up location, *Geophys. Res. Lett.*, **30**(6), 1282, doi:10.1029/2002GL016569, 2003.
- Gérard, J.-C., B. Hubert, M. Meurant, V. I. Shematovich, D. V. Bisikalo, H. Frey, S. Mende, G. R. Gladstone, and C. W. Carlson, Observation of the proton aurora with IMAGE FUV imager and simultaneous ion flux in situ measurements, *J. Geophys. Res.*, **106**, 28,939, 2001.

- Haerendel, G., Disruption, ballooning or auroral avalanche—On the cause of substorms, *Proceedings of the First International Conference on Substorms (ICS-1)*, pp. 417–420, Eur. Space Agency, Kiruna, Sweden, 1992.
- Hones, E. W., Plasma flows in the magnetotail and its implications for substorm theories, *Dynamics of the Magnetosphere*, edited by S. I. Akasofu, pp. 545–562, D. Reidel, Norwell, Mass., 1979.
- Hones, E. W., and K. Schindler, Magnetotail plasma flow during substorms: A survey with IMP 6 and IMP 8 satellites, *J. Geophys. Res.*, **84**, 7155, 1979.
- Hubert, B., J. C. Gérard, D. S. Evans, M. Meurant, S. B. Mende, H. U. Frey, and T. J. Immel, Total electron and proton energy input during auroral substorms: Remote sensing with IMAGE-FUV, *J. Geophys. Res.*, **107**(A8), 1183, doi:10.1029/2001JA009229, 2002.
- Jaqurey, C., J. A. Savaud, and J. Dandouras, Location and propagation of the magnetotail current disruption during substorm expansion: Analysis and simulation of an ISEE multi-onset event, *Geophys. Res. Lett.*, **18**, 389, 1991.
- Kisabeth, J. L., and G. Rostoker, Development of the polar electrojet during polar magnetic substorms, *J. Geophys. Res.*, **76**, 6815, 1971.
- Liou, K., C.-I. Meng, T. Y. Lui, P. T. Newell, M. Brittacher, G. Parks, G. D. Reeves, R. R. Anderson, and K. Kumoto, On relative timing in substorm onset signatures, *J. Geophys. Res.*, **104**, 22,807, 1999.
- Lui, A. T. Y., A synthesis of magnetospheric substorm models, *J. Geophys. Res.*, **96**, 1849, 1991.
- Lui, A. T. Y., C.-L. Chang, A. Mankofsky, H.-K. Wong, and D. Winske, A cross-field current instability for substorm expansions, *J. Geophys. Res.*, **96**, 11,389, 1991.
- Lyons, L. R., Geomagnetic disturbances: Characteristics of, distinction between types, and relations to interplanetary conditions, *J. Atmos. Terr. Phys.*, **62**, 1087, 2000.
- McIlwain, C. E., Substorm injection boundaries, *Magnetospheric Physics*, edited by B. M. McCormac, pp. 143–154, D. Reidel, Norwell, Mass., 1974.
- McPherron, R. L., M. P. Aubry, C. T. Russell, and P. J. Coleman, Satellite studies of magnetospheric substorms on August 15, 1968: IV. Ogo 5 magnetic field observations, *J. Geophys. Res.*, **78**, 3068, 1973.
- Mende, S. B., R. D. Sharp, E. G. Shelley, G. Haerendel, and E. W. Hones, Coordinated observations of the magnetosphere: The development of a substorm, *J. Geophys. Res.*, **77**, 4682, 1972.
- Mende, S. B., et al., Far ultraviolet imaging from the IMAGE spacecraft: 1. System design, 3. Spectral imaging of Lyman- α and O I 135.6 nm, *Space Sci. Rev.*, **91**, 243, 2000.
- Mende, S. B., H. U. Frey, M. Lampton, J.-C. Gérard, B. Hubert, S. Fuselier, J. Spann, R. Gladstone, and J. L. Burch, Global observations of proton and electron auroras in a substorm, *Geophys. Res. Lett.*, **28**, 1139, 2001.
- Mende, S. B., H. U. Frey, T. J. Immel, J.-C. Gérard, B. Hubert, and S. A. Fuselier, Global imaging of proton and electron aurorae in the far ultraviolet, *Space Sci. Rev.*, submitted, 2002.
- Mende, S. B., C. Carlson, H. U. Frey, T. J. Immel, and J.-C. Gérard, IMAGE FUV and in situ FAST particle observations of substorm aurorae, *J. Geophys. Res.*, **108**(A4), 8010, doi:10.1029/2002JA009413, 2003.
- Newell, P. T., Y. I. Feldstein, Y. I. Galperin, and C.-I. Meng, Morphology of nightside precipitation, *J. Geophys. Res.*, **101**, 10,737, 1996.
- Nishida, A., and S. Kokubun, New polar magnetic disturbances: S_q^p, SP, DPC, and DP 2, *Rev. Geophys. Space Phys.*, **9**, 417, 1971.
- Ohtani, S., S. Kokubun, R. C. Elphic, and C. T. Russell, Field aligned current signatures in the near-Earth tail region: 1. ISEE observations in the plasma sheet boundary layer, *J. Geophys. Res.*, **93**, 9709, 1988.
- Ohtani, S., F. Creutzberg, T. Mukai, H. Singer, A. T. Y. Lui, M. Nakamura, P. Prikryl, K. Yumoto, and G. Rostoker, Substorm onset timing: The December 31, 1995, event, *J. Geophys. Res.*, **104**, 22,713, 1999.
- Samson, J. C., L. R. Lyons, P. T. Newell, F. Creutzberg, and B. Xu, Proton aurora and substorm intensifications, *Geophys. Res. Lett.*, **19**, 2167, 1992a.
- Samson, J. C., D. D. Wallis, T. J. Hughes, F. Creutzberg, J. M. Ruohomäki, and R. A. Greenwald, Substorm intensifications and field line resonances in the nightside magnetosphere, *J. Geophys. Res.*, **97**, 8495, 1992b.
- Sergeev, V. A., E. M. Sazhina, N. A. Tsyganenko, J. A. Lundblad, and F. Soraas, Pitch-angle scattering of energetic protons in the magnetotail current sheet as the dominant source of their isotropic precipitation into the nightside ionosphere, *Planet. Space Sci.*, **31**, 1147, 1983.
- Sergeev, V. A., V. Angelopoulos, D. G. Mitchell, and C. T. Russell, In situ observations of magnetotail reconnection prior to the onset of a small substorm, *J. Geophys. Res.*, **100**, 19,121, 1995.
- Shiokawa, K., W. Baumjohann, and G. Haerendel, Braking of high speed flows in the near-Earth tail, *Geophys. Res. Lett.*, **24**, 1179, 1997.
- Shiokawa, K., et al., High-speed ion flow, substorm current wedge, and multiple Pi 2 pulsations, *J. Geophys. Res.*, **103**, 4491, 1998.
- Takahashi, Y., and H. Fukunishi, The dynamics of the proton aurora in auroral breakup events, *J. Geophys. Res.*, **106**, 45, 2001.

C. W. Carlson, H. U. Frey, S. B. Mende, N. Østgaard, and L. M. Peticolas, Space Science Laboratory, University of California, Berkeley, Berkeley, CA 94729, USA. (cwc@ssl.berkeley.edu; hfrey@ssl.berkeley.edu; mende@ssl.berkeley.edu; nikost@ssl.berkeley.edu; lmp@ssl.berkeley.edu)